CrossMark

Field dependence of magnetocaloric properties of 20% Cr-doped $Pr_{0.7}Ca_{0.3}MnO_3$ perovskite

R. M'nassri[1] · A. Selmi[1] · N. Chniba Boudjada[2] · A. Cheikhrouhou[3]

Abstract In this study, we have investigated the effect of 20% Cr doping at the Mn site on the magnetic and magnetocaloric properties of $Pr_{0.7}Ca_{0.3}MnO_3$ polycrystalline manganites elaborated using the solid-state reaction. The X-ray powder diffraction shows that compounds crystallize in the orthorhombic system with Pnma space group. The parent compound $Pr_{0.7}Ca_{0.3}MnO_3$ is a well-known charge-ordered (CO) compound. The selective substitution of Cr for Mn in the pristine compound destroys the CO ordering observed in $Pr_{0.7}Ca_{0.3}MnO_3$, and a paramagnetic to ferromagnetic transition takes place. The field dependence of the magnetic entropy change ΔS and of the relative cooling power RCP is reported. The $|\Delta S^{max}|$ are found to be 0.8 and 2.87 J kg^{-1} K in a magnetic field change of 5 T for $x = 0$ and 0.2, respectively. The RCP is found to be 253.2 J kg^{-1} in the $Pr_{0.7}Ca_{0.3}Mn_{0.8}Cr_{0.2}O_3$ at 5 T. With the scaling laws, the experimental ΔS and n collapse onto a universal curve for $Pr_{0.7}Ca_{0.3}Mn_{0.8}Cr_{0.2}O_3$ sample, where an average curve is obtained for ΔS. With the phenomenological universal curve, the magnetic entropy change ΔS curves are well predicted for Cr-substituted sample. Additionally, Banerjee's criteria, the universal behavior and Landau theory of phase transitions were also studied to assess magnetic ordering in the $Pr_{0.7}Ca_{0.3}Mn_{0.8}Cr_{0.2}O_3$ material.

Introduction

The magnetic cooling based on the magnetocaloric effect (MCE) has been of particular interest due to its high efficiency, compactness and environment-friendly nature compared to the conventional gas refrigeration [1–3]. The major advantages of magnetic refrigeration technology over compressor-based systems are that magnetic refrigeration eliminates toxic gas emission, is a relatively quiet technology (no compressors) and has a higher energy efficiency [4–8]. It offers a green solution to refrigerant fluids such as chlorofluorocarbons, hydrochlorofluorocarbons and ammonia-based compounds. Furthermore, the intrinsic better performance is the reason that this cooling system reduces the electric energy used to run refrigeration units [9–11]. Pr-based manganites have been the subject of extensive study, due to their large magnetocaloric effect (MCE) observed in the wide range of temperature [12–14]. Moreover, these materials present interesting properties such as low cost, good chemical stability, easy preparation and ability to control their magnetic transition temperatures (T_C) close to room temperature by substitutions. This makes these systems particularly promising for magnetic refrigeration [8, 13, 15–17]. The perovskite manganites are strongly correlated systems in which competing interactions give rise to a variety of interesting phenomena including colossal magnetoresistance and magnetocaloric effect [12]. Physical properties in these systems come from the interplay between the charge, orbital, spin and lattice degrees of freedom. These factors can be modified by

✉ R. M'nassri
rafik_mnassri@yahoo.fr

[1] Unité de recherche Matériaux Avancés et Nanotechnologies (URMAN), Higher Institute of Applied Sciences and Technology of Kasserine, Kairouan University, B.P. 471, 1200 Kasserine, Tunisia

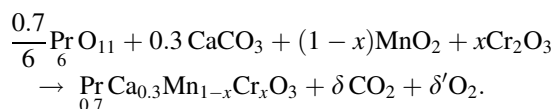[2] Institut NEEL, B.P. 166, 38042 Grenoble Cedex 09, France

[3] Laboratoire of Physics of Materials, Faculty of Sciences of Sfax, Sfax University, B.P. 1171, 3000 Sfax, Tunisia

calcination temperature [18], pressure [19], impurities [20, 21] and particle size [13, 15]. To maintain charge neutrality in doped manganite, the Mn ion exists in two different oxidation states such as Mn^{3+} and Mn^{4+}. The mixed valence introduces mobile electrons leading to a quasi-metallic conductivity and the ferromagnetic ground state in these compounds. This behavior is usually interpreted by means of double-exchange (DE) interaction [22], Jahn–Teller effect [23] and phase separation [24]. The magnetic coupling between Mn^{3+} and Mn^{4+} ions results from the motion of an electron between the two partially filled d orbitals with strong on-site Hund's coupling [25]. Since the magnetic property is dependent on the strength of double-exchange interaction between Mn^{3+} and Mn^{4+} via oxygen, the doping at the A-site is of great importance in modifying the double-exchange strength [26]. Recently, many manganites concerning second-order magnetic transition have been studied in an attempt to achieve a large magnetocaloric effect. The origin of the observed MCE is based on the adiabatic demagnetization: The application of a magnetic field in a ferromagnetic material induces a spin reorientation leading to decrease in the spin entropy. This process is accompanied by a rise of the lattice entropy when the field is applied adiabatically. The strong coupling between the spin and lattice has been shown by the observed lattice changes accompanying magnetic transitions in these manganites; the lattice structural change in the Mn–O bond distances and Mn–O–Mn bond angles with temperature which exhibit variation in the volume can cause an additional change in the magnetism [12, 27]. In $Pr_{1-x}Ca_xMnO_3$ materials, the so-called CE-type charge/orbital-ordered (CO) state is stabilized. Even so, a FM state can be obtained by applying a magnetic field or by a small quantity of Mn substitution by means of other 3d transition metal elements like Fe^{3+}, Co^{3+}, Ni^{3+}, Ru^{3+}, Al^{3+} and Cr^{3+} [14, 28–31]. However, the Cr substitution is particularly interesting as Cr^{3+} is isoelectronic with Mn^{4+} and is a non-Jahn–Teller ion [32]. A literature overview highlights that the ionic radius of chrome ion is near to that of manganese ion, and thus, it can easily substitute Mn on B-site in the manganites system. Much investigation was focused on the structure, electrical and magnetic properties performance of Cr-doped manganites. Indeed, Cr doping in the Mn site is an effective way to change the Mn^{3+}–O–Mn^{4+} network, because it will affect remarkably the double exchange and, consequently, it will change the final physical properties of the material [28]. Therefore, one might expect to induce a ferromagnetic phase in an otherwise antiferromagnetic, charge-ordered ground state. In fact, a ferromagnetic phase has been observed to coexist with the CO phase in Cr-substituted $Pr_{0.5}Ca_{0.5}MnO_3$ for low Cr concentrations at low

temperatures. The results account for the replacement of Mn^{3+} by Cr^{3+}, which makes more disorder in the compound, resulting in an increase in the disorder parameter and the fluctuation of the spin. This raison indicates that the chromium substitution at Mn site alters magnetic response in the sample. So, the effect of substitution on the parent material has been the interesting subject for the systematic study of various characteristics like structural and magnetocaloric behavior [33]. In order to continue our investigation in the Pr-based manganites, we report in this paper the field dependence of Cr doping on magnetic and magnetocaloric properties of $Pr_{0.7}Ca_{0.3}Mn_{1-x}Cr_xO_3$.

Experimental

Ceramic materials with the nominal composition of $Pr_{0.7}Ca_{0.3}MnO_3$ ($x = 0.0$) and ($x = 0.2$) samples were synthesized from high-purity precursors: Pr_6O_{11}, $CaCO_3$, Cr_2O_3 and Mn_2O_3 (Aldrich 99.9%; USA) by the conventional solid-state reaction method at high temperature. Stoichiometric ratios of starting chemicals precursors were taken and thoroughly mixed for 35 min using an agate mortar. The obtained powders were then pressed into cylindrical shape of diameter 10 mm using a hydraulic press by applying a pressure of 2 tons cm^{-2} and grounded and pre-annealed at 800, 1000, 1100 and 1300 °C for 24 h (heating rate of the order 10 °C per minute was used) for each cycle to ensure a better crystallization according to the following reaction [34]:

$$\frac{0.7}{6}Pr_6O_{11} + 0.3\,CaCO_3 + (1-x)MnO_2 + xCr_2O_3$$
$$\rightarrow Pr_{0.7}Ca_{0.3}Mn_{1-x}Cr_xO_3 + \delta\,CO_2 + \delta'O_2.$$

The obtained disk-shaped samples were cooled from high temperature to room temperature following the cooling inertia of the furnace (~ 8 h). As both samples have been elaborated in air, they are consequently stoichiometric in oxygen [35, 36]. Phase purity, homogeneity and cell dimensions were determined by powder X-ray diffraction at room temperature for both samples. The room temperature X-ray diffraction (XRD) patterns were measured by a PANalytical X'PERT Pro MPD diffractometer, using $\theta/2\theta$ Bragg–Brentano geometry with diffracted beam monochromatized Cu Kα radiation. The diffraction patterns were collected by steps of 0.017° over the angle range 10°–80°. Structural analyses were carried out by the standard Rielveld method [37, 38] using Fullprof software. Magnetization measurements versus temperature in the range 5–300 K and versus magnetic applied field up to 5 T were taken using a vibrating sample magnetometer. Magnetocaloric results were deduced from the isothermal magnetization measurements.

Results and discussion

X-ray diffraction analysis

The results of the XRD studies at room temperature of $Pr_{0.7}Ca_{0.3}MnO_3$ and $Pr_{0.7}Ca_{0.3}Mn_{0.8}Cr_{0.2}O_3$ materials show that our samples crystallize in the orthorhombic system with the Pnma space group. The atoms (Pr, Ca) are located at 4c (x, 1/4, z), (Mn, Cr) at 4b (1/2, 0, 0), O_1 at 4c (x, 1/4, z) and O_2 at (x, y, z). Figure 1 shows a typical Rietveld refinement for both samples registered at 300 K including the observed and calculated profiles as well as the difference profile. The quality of the refinement is evaluated through the goodness of the fit indicator χ^2 (1.21 for $x = 0.0$ and 1.41 for $x = 0.2$). A good fit between the observed and the calculated profiles was obtained. The cell parameters for $Pr_{0.7}Ca_{0.3}MnO_3$ are found to be $a = 5.459(8)$ Å, $b = 7.674(1)$ Å and $c = 5.430(3)$ Å. For 20% Cr-doped manganite, they are found to be $a = 5.426(4)$ Å, $b = 7.666(8)$ Å and $c = 5.446(4)$ Å. One may remark that the volume decreases from 227.52 to 226.58 Å^3 with the replacement of partial Mn ions by Cr ions. This can be explained by the difference in the ionic radii between the larger Mn^{3+} ions (0.65 Å) which substituted for the smaller Cr^{+3} (0.61 Å) in B sites. It is noticed that for 20% Cr substitution, the average distances of Mn–O drop from 1.970(1) to 1.959(1) Å, and the average angles of Mn–O–Mn jump from 157.55(4)° to 159.89(8)°. However, chromium ions with smaller ionic radius induce local distortions of the ⟨Mn–O–Mn⟩ angle in the system. The internal stress caused by substituting Mn^{3+} by Cr^{3+} may result in a larger rotation of the MnO_6 octahedra [39]. These modifications can be understood on the basis of structural parameters, B-site average ionic radius '$<r_B>$,' B-site size variance 'σ_B^2' and tolerance factor 't'.
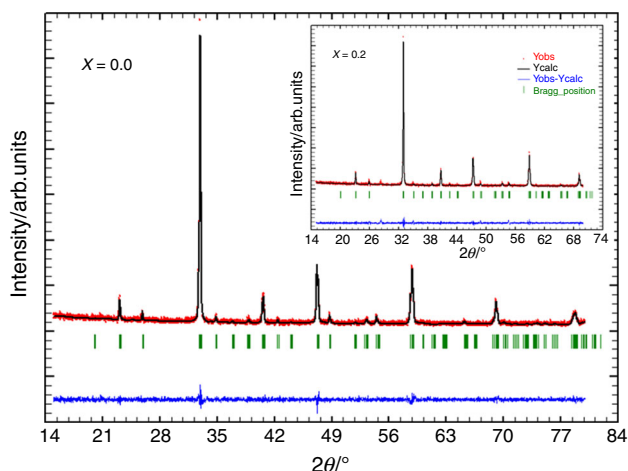
Mainly, the remarkable observation from the XRD data was that the principal diffraction peak position of $Pr_{0.7}Ca_{0.3}MnO_3$ shifted toward higher diffraction angle with Cr substitution, which confirms that the unit cell volume decreases with the doping of Cr. Thus, the lattice structural change, which results in a variation of the volume, can cause an additional change in the magnetic properties of the material.

Magnetic properties

We plot in the inset of Fig. 2 the low field ($\mu_0 H = 0.05$ T) temperature dependence of the magnetization $M(T)$ for the pristine compound. The measurements were taken after field cooling (FC) process. A signature of anomaly can be observed in the $M(T)$ curve around 250 K, associated with the charge-ordering state (ordering of electrons and holes of Mn^{3+} and Mn^{4+} ions, respectively). This behavior is promoted by the cooperative Jahn–Teller ordering of, for example, orbitals. At $T \sim 100$ K, the rapid increase in $M(T)$ in this compound is generally attributed to polarization of the Pr moments. Figure 2 shows the field dependence of magnetization measurements versus magnetic applied field at several temperatures. At low temperature, the $M(\mu_0 H)$ of $Pr_{0.7}Ca_{0.3}MnO_3$ increases linearly up to $\mu_0 H = 3.2$ T and then shows a rapid increased metamagnetic transition due to the progressive conversion of the charge-ordered (CO) state into a ferromagnetic behavior [40]. At high temperature, magnetization curves completely become linear with magnetic field as expected for the paramagnetic state. In our work, the chromium substitution is established to destroy the charge ordering observed in the parent compound and to drive the system toward a ferromagnetic state at low temperatures.
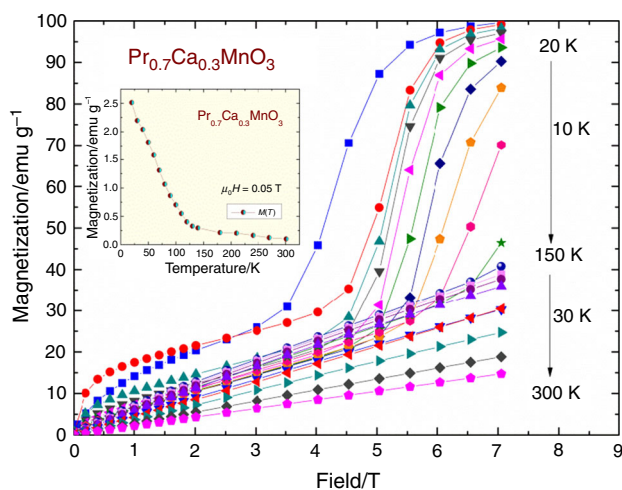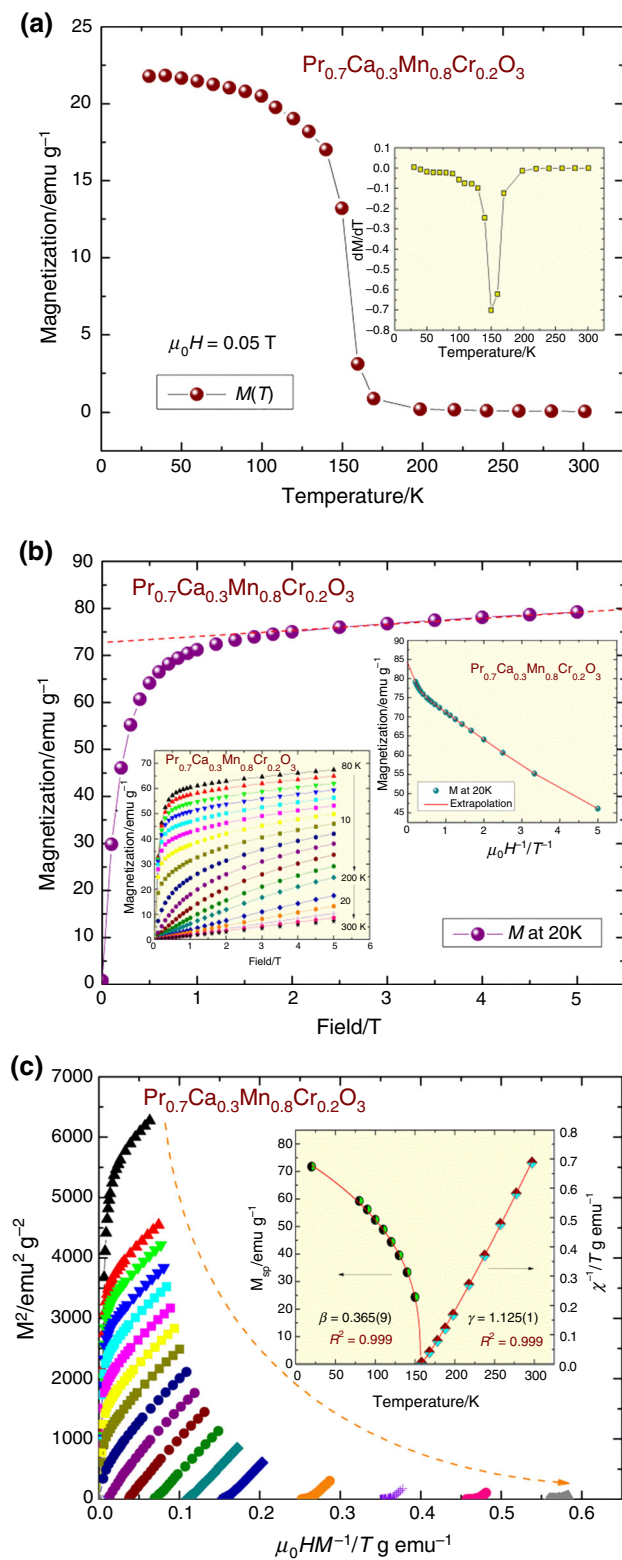

Fig. 1 X-ray powder diffraction patterns and refinement at room temperature for $Pr_{0.7}Ca_{0.3}Mn_{1-x}Cr_xO_3$ ($x = 0$ and $x = 0.2$)

Fig. 2 Isothermal magnetization curves at various temperatures for $Pr_{0.7}Ca_{0.3}MnO_3$. The *inset* is the temperature dependence of magnetization under 0.05 T for $Pr_{0.7}Ca_{0.3}MnO_3$ compound

(a)

(b)

(c)

Fig. 3 a Temperature dependence of magnetization under 0.05 T for $Pr_{0.7}Ca_{0.3}Mn_{0.8}Cr_{0.2}O_3$ compound. The *inset* is the dM/dT curves. **b** Magnetization versus magnetic applied field at 20 K for $Pr_{0.7}Ca_{0.3}Mn_{0.8}Cr_{0.2}O_3$. The *insets* determination of the saturation magnetization of the samples at 20 K and isothermal magnetization curves at various temperatures for $Pr_{0.7}Ca_{0.3}Mn_{0.8}Cr_{0.2}O_3$. **c** M^2 versus $\mu_0 H/M$ isotherms for $Pr_{0.7}Ca_{0.3}Mn_{0.8}Cr_{0.2}O_3$. The *inset* is the temperature dependence of the spontaneous magnetization M_{sp} and $1/\chi$ for $Pr_{0.7}Ca_{0.3}Mn_{0.8}Cr_{0.2}O_3$

sample exhibits a clear transition from paramagnetic to ferromagnetic state with decreasing temperature. The replacement of Mn^{3+} by 20% Cr^{3+} introduces a diminution of the Mn^{3+} ion concentration which decreases the Mn^{3+}/Mn^{4+} ratio, changes both the average bond length $\langle Mn–O \rangle$ and angle $\langle Mn–O–Mn \rangle$ and influences ferromagnetic interaction strengths [41]. This effect has a direct impact on the double-exchange (DE) interactions. Also, it affects other mechanisms such as ferromagnetic interactions and antiferromagnetic super-exchange which are possible to occur between Cr and Mn ions. Here, the main role of the Cr^{3+} ion is to polarize the Mn^{3+} ions. Consequently, these factors lead to a second-order magnetic phase transition in this compound and reveal a strong variation of magnetization around the Curie temperature T_C. The derivative dM/dT of the $M(T)$ curve is used to determine the value of Curie temperature $T_C \sim 155$ K. The dM/dT curve reveals a strong variation of magnetization around the T_C. It indicates that there is a possible large magnetic entropy change around T_C [42].

To understand the nature of the magnetic order fluctuations in our samples, we measured the field dependence of isothermal magnetization at several temperatures. The inset of Fig. 3b shows isothermal magnetization curves for the $Pr_{0.7}Ca_{0.3}Mn_{0.8}Cr_{0.2}O_3$ sample. This plots show clearly the evolution of our material at low temperatures from the CO state in the undoped compound to the ferromagnetic state in the substituted sample. For Cr-doped system and below T_C, the $M(\mu_0 H)$ curves increase sharply for magnetic field <1 T and tend to saturation. This result confirms well the ferromagnetic behavior at low temperature of our material. It can be expected that the Cr substitution at the Mn sublattices is a disorder effect, which can disrupt the cooperative Jahn–Teller ordering of, for example, orbitals, which in turn can lead to destabilization of the CO state [43, 44]. We plot in Fig. 3b the magnetic isotherm at 20 K for $Pr_{0.7}Ca_{0.3}Mn_{0.8}Cr_{0.2}O_3$. The obtained curve was used for evaluation of the characteristic magnetization values by means of procedures described in [45]. Namely, the saturations magnetizations M_{sat} at 20 K was calculated from M versus $1/\mu_0 H$ plot at $1/\mu_0 H \rightarrow 0$ (see inset of Fig. 3b). The obtained values of $M_{sat} = 84.15$ emu g^{-1} were of the same order as that of $Pr_{0.7}Ca_{0.3}Mn_{0.95}X_{0.05}O_3$(X = Cr, Ni, Co and Fe) [14], $Pr_{0.5}Eu_{0.1}Sr_{0.4}MnO_3$ [13] and $La_{0.85}Ag_{0.15}Mn_{1-y}M_yO_3$ [46]. At low temperature, the spontaneous

To recall the characteristic magnetic behavior of $Pr_{0.7}Ca_{0.3}Mn_{0.8}Cr_{0.2}O_3$ system, the M-T measurement employing the field-cooled (FC) protocol at 0.05 T in the temperature range of 5–300 K is shown in Fig. 3a. The

magnetization M_{sp}(exp) determined by the extrapolation of the M versus μ_0H data in the high field to zero field is found to be 72.55 emu g^{-1} ($\sim$2.77μ_B/Mn) (see Fig. 3b). The magnitude of the M_{sp}(exp) is smaller than the theoretical value of 3.5 μ_B/Mn calculated for full spin alignment, leading to small canted spins. This result confirms the existence of the antiferromagnetic (AFM) interactions and signifying that the magnetic moment of the rare-earth ions are polarized and pinned by the Mn sublattice [47, 48]. The order of the transition in Cr-doped manganite is clarified by Banerjee criterion [49]. This criterion suggests a magnetic transition of first order with negative slopes and a second-order transition with positive slopes. Figure 3c shows the Arrott plots (M^2 vs μ_0H/M) for Pr$_{0.7}$Ca$_{0.3}$Mn$_{0.8}$Cr$_{0.2}$O$_3$ sample. The M^2 versus μ_0H/M curves exhibit a positive slope without inflection points, indicating that the ferromagnetic–paramagnetic transition is of second order [50]. It can be mentioned that Arrott plot assumes the critical exponents following the mean field theory ($\beta = 0.5$ and $\gamma = 1$). Hence, linear behavior of isotherms in high field indicates the presence of mean field interactions. The advantages of this plot are (1) T_C can be determined accurately since the isotherm at T_C will pass through the origin, (2) it gives spontaneous magnetization $M_{sp}(T)$ as intercept on positive M^2 axis, and (3) it directly gives the inverse of the magnetic susceptibility χ^{-1} versus T as an intercept on μ_0H/M axis. The T_C value deduced from the Arrott curves is close to this determined from $M(T)$ curve. The inset of Fig. 3c shows the temperature dependence of the spontaneous magnetization M_{sp} and the inverse of the magnetic susceptibility χ^{-1} evolution versus temperature for Pr$_{0.7}$Ca$_{0.3}$Mn$_{0.8}$Cr$_{0.2}$O$_3$. The $M_{sp}(T)$ curve confirms the FM behavior of chromium-substituted material at low temperatures. The critical exponents β and γ are defined by:

$$M_{sp}(T) = M_{sp}(0)\left[1 - \frac{T}{T_C}\right]^{\beta} \text{ and } \chi^{-1}(T)$$
$$= \chi^{-1}(0)\left[\frac{T}{T_C} - 1\right]^{\gamma} \tag{1}$$

The estimated values of the critical exponents for Pr$_{0.7}$Ca$_{0.3}$Mn$_{0.8}$Cr$_{0.2}$O$_3$ sample associated with the spontaneous magnetization and the inverse of the magnetic susceptibility are found to be $\beta = 0.365(9)$ and $\gamma = 1.125(1)$. Fundamentally, β keeps close to the value expected for the 3D Heisenberg ferromagnets with ferromagnetic short-range interactions, while γ is near the critical value of the mean field theory. Basically, the determined value of δ will be close to that calculated from the Widom relation $\delta = 1 + \gamma/\beta = 4.074(8)$. These values of critical exponents are between the predicted values for the three-dimensional Heisenberg model ($\beta = 0.37$, $\gamma = 1.39$,

$\delta = 4.7$) and for the mean field model ($\beta = 0.5$, $\gamma = 1$, $\delta = 3$) as observed in other manganites [51, 52].

Magnetocaloric effect

The isothermal magnetization curves are used to determine the magnetic entropy change ΔS of our samples under a magnetic applied field change $\Delta\mu_0H$ according to the classical thermodynamic theory based on Maxwell's relations using the following expression:

$$\Delta S(T, \mu_0H) = \sum \left(\frac{M_i - M_{i+1}}{T_{i+1} - T_i}\right)\Delta\mu_0H_i \tag{2}$$

In this equation, M_i and M_{i+1} are the experimental values of magnetization measured at temperatures T_i and T_{i+1}, respectively, under magnetic applied field μ_0H_i. Experimentally, the ΔS is often evaluated by some numerical approximation methods. One is to use directly the measurements of M–T curve under different applied magnetic fields. Another method is estimation through either the adiabatic change in temperature (ΔT_{ad}) by the application of a magnetic field or isothermal magnetization measurements at several temperatures. In this work, we have used the third method based on magnetization measurements versus a magnetic applied field. Figure 4a depicts the magnetic entropy change as a function of temperature at several magnetic fields for the undoped compound. Pr$_{0.7}$Ca$_{0.3}$MnO$_3$ material exhibits a positive entropy change due to the dominance of the antiferromagnetic interactions with a maximum value of 0.8 J kg^{-1} K upon a magnetic field change of 5 T. The substitution of Mn^{3+} by 20% Cr^{3+} introduces a diminution of the Mn^{3+} ion concentration which changes both the average bond length $\langle$Mn–O$\rangle$ and angle $\langle$Mn–O–Mn$\rangle$ and influences MCE properties. Figure 4b shows the magnetic entropy change ΔS evolution as a function of temperature of Pr$_{0.7}$Ca$_{0.3}$Mn$_{0.8}$Cr$_{0.2}$O$_3$ sample. The ΔS exhibit a broad negative peak around T_C (indicating a ferromagnetic behavior) for the substituted material. For $\Delta\mu_0H = 2$ T and 5 T, the maximum magnetic entropy change $|\Delta S^{max}|$ is found to be 1.5 and 2.87 Jkg^{-1} K^{-1}, respectively. In particular, the magnetic entropy change in the Cr-doped sample demonstrates a significant broad variation with temperature around T_C. Such variation covering a broad temperature range is beneficial for magnetic cooling applications [53]. This is a very interesting result, because we are able to change MCE and width of peak temperature range of the material by substituting manganese ion and may select optimization, which is desirable for Ericsson-cycle magnetic refrigeration and heat exchange technology [2]. In the magnetic cooling technology, it is important that the magnetocaloric effect (MCE) extends over a large temperature range. We can then consider the magnitude of
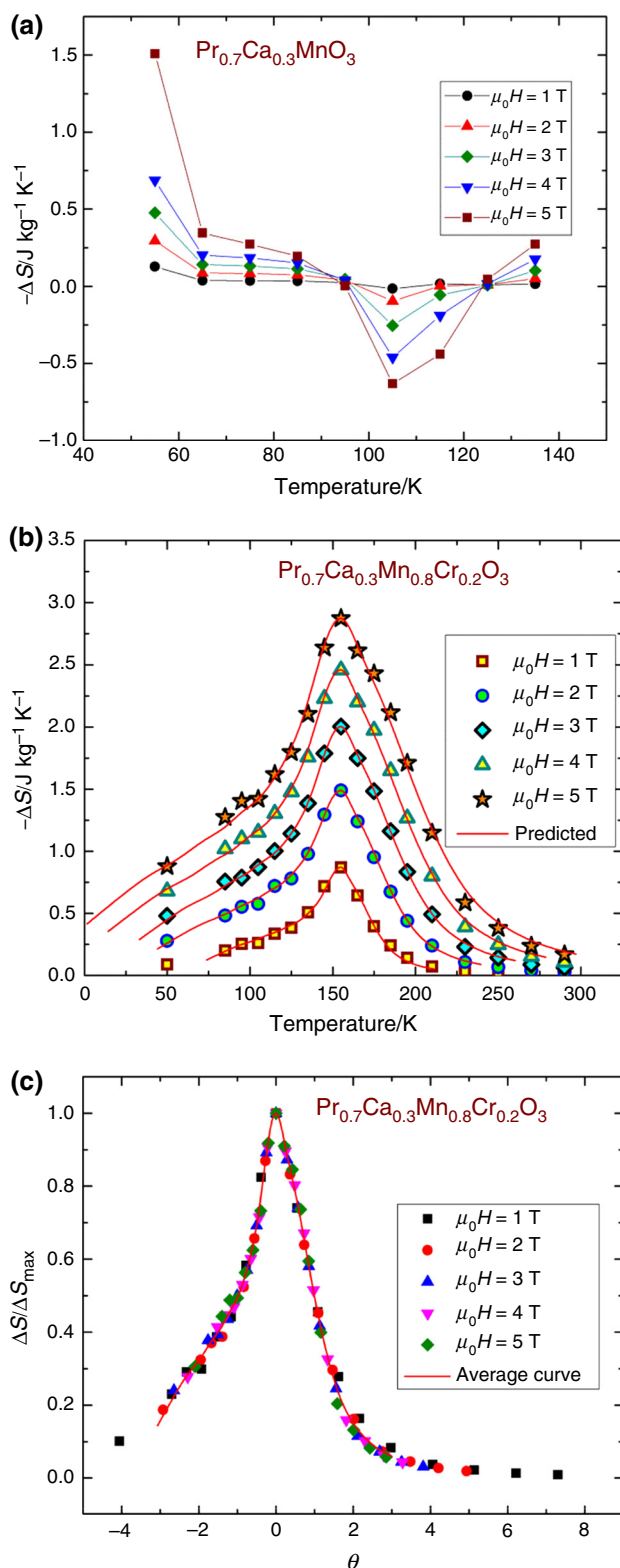
Fig. 4 a Magnetic field dependence of magnetic entropy change for $Pr_{0.7}Ca_{0.3}MnO_3$. **b** Experimental (*open symbols*) magnetic entropy change and predictions using the universal curve (*continuous lines*) for $Pr_{0.7}Ca_{0.3}Mn_{0.8}Cr_{0.2}O_3$. **c** The collapse of the experimental data onto the universal curve for $Pr_{0.7}Ca_{0.3}Mn_{0.8}Cr_{0.2}O_3$

ΔS and its full width at half maximum, known as the relative cooling power (RCP) [12]. The RCP is evaluated as $RCP = \left| \Delta S_M^{max}(T, H) \right| \times \delta T_{FWHM}$. The obtained value of RCP for $Pr_{0.7}Ca_{0.3}Mn_{0.8}Cr_{0.2}O_3$ is found to be 253.2 J kg^{-1} at 5 T. In Table 1, we have compared the entropy changes in our sample with other B-site multi-element doping effect like Cr, Ni and Fe in several manganites system. The obtained values are comparable with those mentioned in Table 1. All these studies indicate that the large MCE in the perovskite manganites can originate from the spin-lattice coupling related to the magnetic ordering process. The lattice structural change in B–O bond distances and B–O–B, bond angles with temperature, which results in a variation of the volume, can cause an additional change in the magnetic properties of manganite.

Currently, a phenomenological construction of universal curve for $\Delta S(T)$ has been proposed as a method to compare the properties of several magnetic materials and to make extrapolations to fields and/or temperatures outside the available experimental range [61]. It is interesting to note that the collapse of these curves is observed not only in the near vicinity of the transition but in a wide temperature range. This raises the question as to whether the collapse of the $\Delta S(T)$ curves is a manifestation of a universal behavior or not. A study on first-order phase transitions should shed light on the subject: A breakdown of the universal curve is expected for first-order phase transitions if the underlying cause is universality associated with critical phenomena and intrinsic to second-order phase transitions. Otherwise, $\Delta S(T)$ curves may collapse in the same way for first-order as for second-order transitions. The magnetocaloric universal behavior of $Pr_{0.7}Ca_{0.3}Mn_{0.8}Cr_{0.2}O_3$ is studied as a verification of Banerjee criterion [49]. This new criterion based on the entropy changes can be helpful in distinguishing the order of magnetic phase transitions. For ferromagnets undergoing second-order phase, the rescaled magnetic ΔS curves follow a universal behavior. While the scaled ΔS curves do not collapse as a single curve, the ferromagnets undergo a first-order phase transition. The phenomenological universal curve can be constructed by normalizing and rescaling the temperature axis below and above T_C as defined in Eq. (3) with an imposed constraint that the position of two additional reference points in the curve corresponding to $\theta \pm 1$. This procedure is used to compare the properties of several materials and to make extrapolations to temperatures and/or fields outside the accessible experimental range. A way of doing this would be to normalize all ΔS curves with their peak entropy change, respectively, as $\Delta S' = \Delta S/2$, and the temperature axis is rescaled by a new term denoted by θ and is given as below [7, 62]:

Table 1 T_C, ΔS_{max} and RCP values for the present samples under a magnetic applied field of 5 T and for some previous works

Materials	T_C/K	$\Delta \mu_0 H$/T	ΔS_{max}/Jkg^{-1} K^{-1}	RCP/J kg^{-1}	References
$Pr_{0.6}Ca_{0.1}Sr_{0.3}Mn_{0.95}Fe_{0.05}O_3$	185	5	3.70	233	[54]
$La_{0.6}Pr_{0.1}Ba_{0.3}Mn_{0.7}Ni_{0.3}O_3$	131	5	0.65	62	[55]
$La_{0.7}Sr_{0.3}Mn_{0.8}Fe_{0.2}O_3$	94	5	1.3	168	[56]
$La_{0.7}Sr_{0.3}Mn_{0.9}Fe_{0.1}O_3$	260	5	3.1	192	[56]
$La_{0.67}Sr_{0.33}Mn_{0.9}Cr_{0.1}O_3$	328	5	5	200	[57]
$Nd_{0.67}Ba_{0.33}Mn_{0.98}Fe_{0.02}O_3$	134	5	2.97	242	[58]
$La_{0.67}Ca_{0.33}Mn_{0.75}Cr_{0.25}O_3$	193	5	2.2	88	[59]
$La_{0.67}Ba_{0.33}Mn_{0.9}Cr_{0.1}O_3$	324	5	4.2	238	[60]
$Pr_{0.7}Ca_{0.3}Mn_{0.8}Cr_{0.2}O_3$	155	5	2.87	253.2	Present

$$\theta = \begin{cases} -(T - T_C)/(T_{r1} - T_C); & T \leq T_C \\ (T - T_C)/(T_{r2} - T_C); & T > T_C \end{cases} \quad (3)$$

where T_{r1} and T_{r2} are the temperatures of the two reference points of each curve that correspond to $\Delta S/2$. The universal curves of $Pr_{0.7}Ca_{0.3}Mn_{0.8}Cr_{0.2}O_3$ at several magnetic fields are constructed in Fig. 4c. It is seen that all curves collapse onto a single master curve revealing second-order phase transition in this compound which confirms the result obtained by Banerjee criterion. The average curve is obtained from the universal scaling, as shown as solid curve in Fig. 4c which gives a smoother depiction of the curve. The mentioned curve, once the temperature axis is backtransformed from the reduced temperature to the unnormalized one, allows making extrapolations to lower/higher temperatures for the high field data and obtaining a finer description of the peak for the low field curves [63, 64]. The combination of all data in the average universal curve and the inverse transformation of the experimental $\Delta S(T)$ axes permits to provide a prediction about the behavior of the curve. The good agreement between predicted and experimental points is remarkable. The predicted curves are given as red solid curves for comparison. A comparison between both curves is presented in Fig. 4b for Cr-substituted material.

The change in specific heat associated with a magnetic field variation from zero to $\mu_0 H$ can be calculated from the magnetic contribution to the entropy change induced in the materials, ΔC_P, by the following expression:

$$-\Delta C_P = T \frac{\partial \Delta S_M}{\partial T} \quad (4)$$

Through this relation, ΔC_P of $Pr_{0.7}Ca_{0.3}Mn_{0.8}Cr_{0.2}O_3$ material versus temperature at several magnetic fields is depicted in Fig. 5. As the figure shows anomalies are observed in all curves around T_C, which are due to the magnetic phase transition [20, 65, 66]. The magnitude of ΔC_P varies abruptly from (+) to (−) near the Curie temperature and speedily decreases with decreasing

temperature. The sum of the two parts is the magnetic contribution to the total specific heat which affects the cooling or heating power of the magnetic refrigerator [67]. Specific heat presents the advantage of delivering values necessary for further refrigerator design, should the material in question be selected [68].

It has also been demonstrated that the field dependence of the maximum magnetic entropy change shows a power law $\Delta S^{max} \approx a(\mu_0 H)^n$ for some materials [53, 61]. In order to check the validity of n value, the experimental data of field dependence of $-\Delta S$ at T_C for $Pr_{0.7}Ca_{0.3}Mn_{0.8}Cr_{0.2}O_3$ sample are plotted in Fig. 6a. The fitting value of n is about 0.781(9) which is significantly higher than 2/3, as predicted by the mean field model. The field dependence of the RCP for the Cr-doped manganite is analyzed. In addition, the magnetic field dependence of the RCP is shown in Fig. 6b. It can be expressed as a power law by taking account of the field dependence of entropy change ΔS and reference
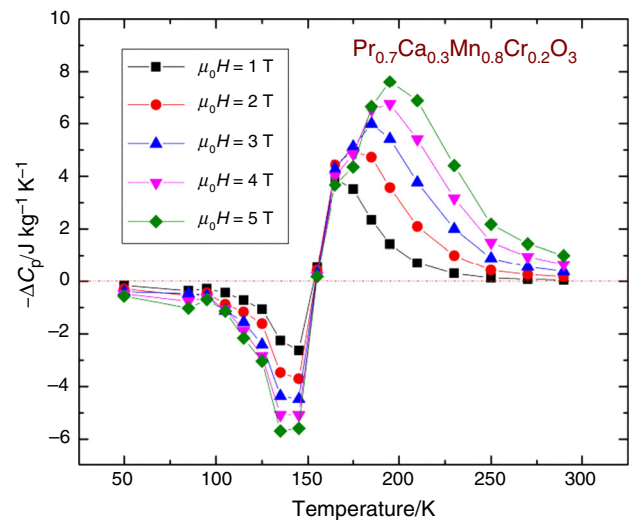
Fig. 5 Heat capacity changes $-\Delta C_p$ as function of temperature for $Pr_{0.7}Ca_{0.3}Mn_{0.8}Cr_{0.2}O_3$

temperature into consideration, i.e., $RCP \approx A(\mu_0 H)^N$ where N is the critical exponent of the magnetic transition. RCP should scale with field as a power law with an exponent N. The N value calculated from experimental data is $N = 1.138(7)$ for our material. This N result is compatible with values previously reported for (Na, K)-doped $Pr_{0.6}Sr_{0.4}MnO_3$ [69, 70] and those observed for Gd alloys ($N = 1.16$) by Law et al. [71]. Refrigerants with a wide working temperature span and high RCP are in fact very beneficial to magnetic cooling applications [5]. The polycrystalline $Pr_{0.7}Ca_{0.3}Mn_{0.8}Cr_{0.2}O_3$ manganite is particularly pronounced with wide operative temperature range, as well as inexpensiveness and easy fabrication, and therefore could be considered as a potential magnetic cooling [16, 72].

Moreover, the n exponent can be locally calculated from the logarithmic derivative of the ΔS with magnetic field as [71]:

$$n(T, \mu_0 H) = \frac{d \ln(|\Delta S|)}{d \ln(\mu_0 H)} \tag{5}$$

given $n = 1$ in the ferromagnetic range for $T \ll T_C$, $n = 2$ in the paramagnetic range for $T \gg T_C$ and $n(T_C) = 1 + \left[\frac{\beta - 1}{\beta + \gamma}\right]$ at $T = T_C$. According to the mean field approach, $n = 2/3$. However, current experimental result reveals deviation from $n = 2/3$ in the case of some ferromagnetic materials [61]. Figure 7a depicts the temperature dependences of the local exponent n for several values of $\mu_0 H$ describing the field dependence of the magnetic entropy change calculated from Eq. (5) when fields of different values are applied. It has to be noted that n evolves with field in the entire studied temperature range. However, $n(T, \mu_0 H)$ plots show the minima around the Curie temperature. The minimum value of n reaches 1 $T \ll T_C$ and 2 $T \gg T_C$.
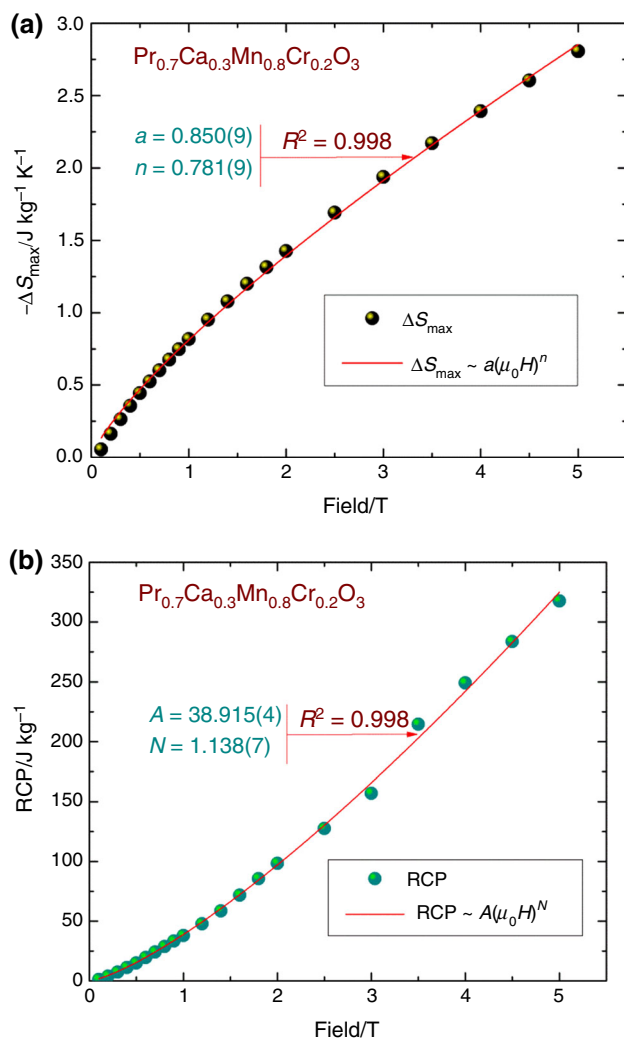

Fig. 6 Magnetic field dependence of: **a** magnetic entropy change ΔS_{max} and **b** RCP for $Pr_{0.7}Ca_{0.3}Mn_{0.8}Cr_{0.2}O_3$
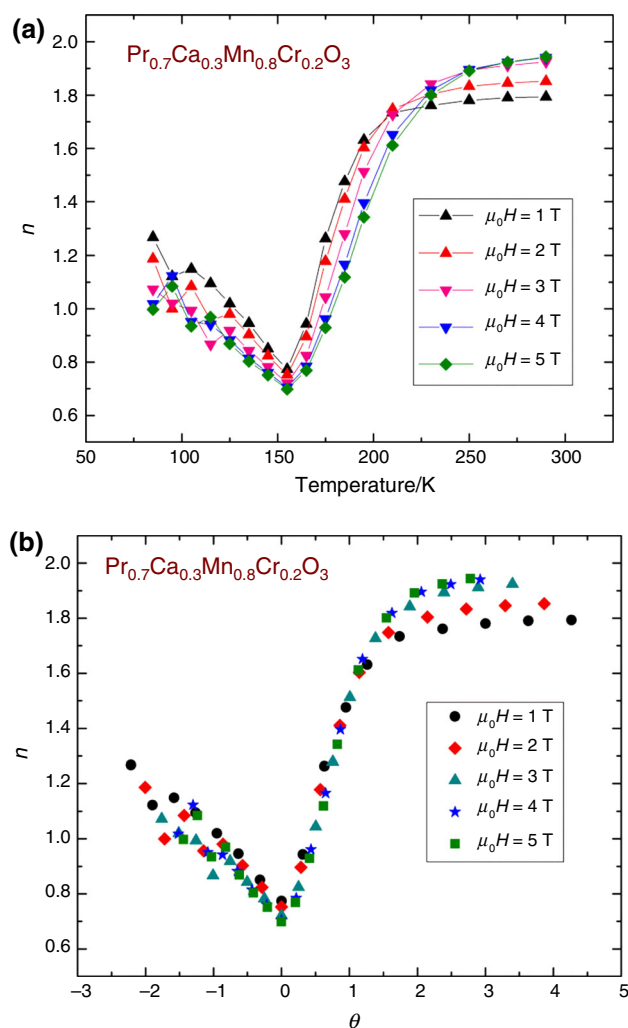
Fig. 7 a Local exponent n at several magnetic fields for $Pr_{0.7}Ca_{0.3-}Mn_{0.8}Cr_{0.2}O_3$ compound. **b** Local exponent n as a function of the rescaled temperature θ for all magnetic fields

In fact, in the present case the value of n at T_C is greater than the predicted value of 2/3 in the mean field approach due to the local inhomogeneities or super-paramagnetic clusters in the vicinity of a transition temperature T_C existed in the $Pr_{0.7}Ca_{0.3}Mn_{0.8}Cr_{0.2}O_3$ specimen [73]. A similar behavior has been observed in $La_{0.7}Ca_{0.3}Mn_{0.91}Ni_{0.09}O_3$ system [74].

The $n(T, \mu_0 H)$ curves also collapse when plotted against the same rescaled temperature axis for which the normalized values of $-\Delta S(T)$ collapse onto the universal curve. The procedure consists of identifying the reference temperatures as those which have a certain value of n. This value has been arbitrarily selected as $n(Tr) = 1.5$. The transformed curves of different fields are plotted in Fig. 7b. This figure shows the rescaled temperature θ dependence of the exponent n for the $Pr_{0.7}Ca_{0.3}Mn_{0.8}Cr_{0.2}O_3$ compound. For several magnetic fields, all the data points collapse into a single master curve revealing universal behavior in $Pr_{0.7}Ca_{0.3}Mn_{0.8}Cr_{0.2}O_3$. In general, deviations

from the collapse might indicate either the influence of the demagnetizing field associated with the shape of the sample [75] or to the presence of additional magnetic phases [76].

The observed $\Delta S(T)$ in La-based manganites have been fitted with models based on Weiss molecular mean field theory or Landau theory of phase transition. It was found that the Landau's theory fits the $\Delta S(T)$ data very closely. Hence, we have attempted to fit the $\Delta S(T)$ data of $Pr_{0.7}Ca_{0.3}Mn_{0.8}Cr_{0.2}O_3$ sample to the Landau theory using the Gibbs free energy following:

$$G(M,T) = G_0 + \frac{1}{2}A \times M^2 + \frac{1}{4}B \times M^4 + \frac{1}{6}C \times M^6 - M\mu_0 H \quad (6)$$

where $A(T)$, $B(T)$ and $C(T)$ are temperature dependent usually known as Landau coefficients.

In order to retain the state of energy minimization in Eq. (6), the magnetic equation of the state is given as
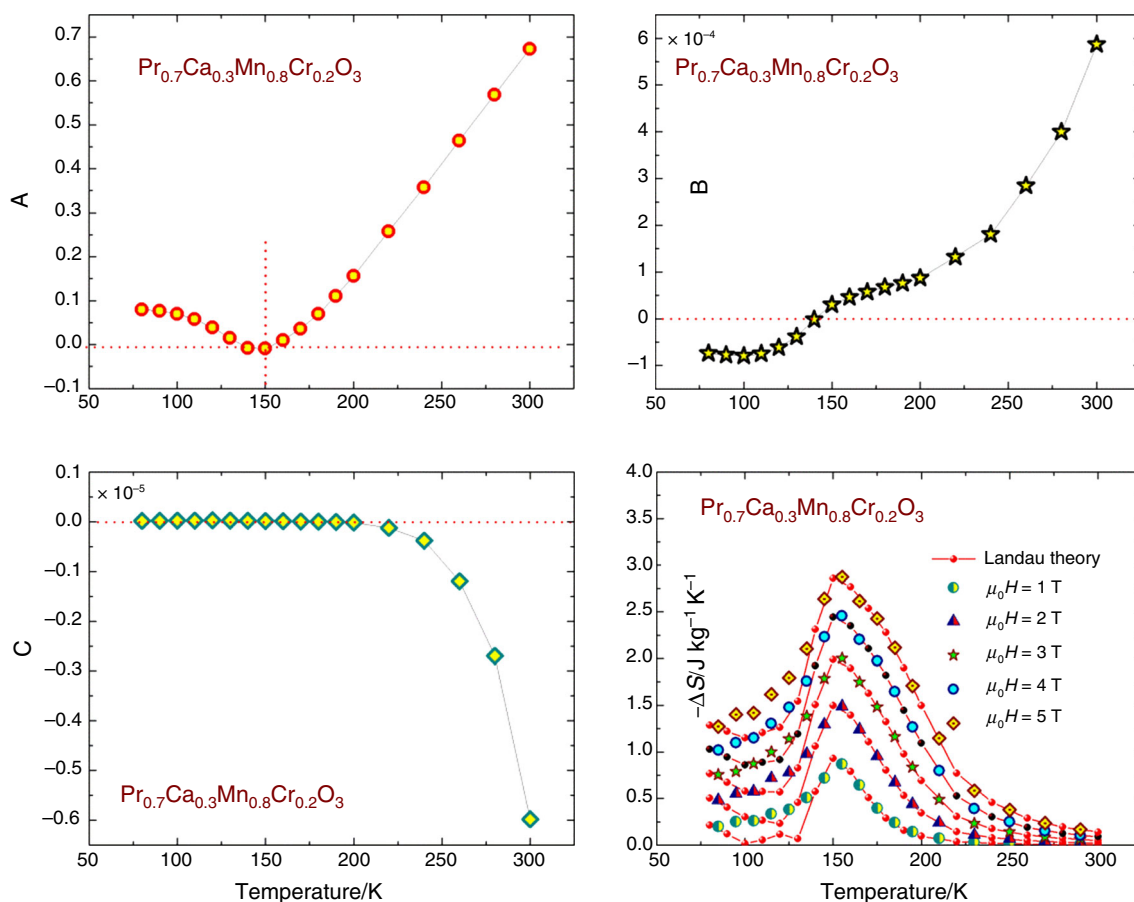

Fig. 8 Temperature dependence of the Landau coefficients $A(T)$, $B(T)$ and $C(T)$ for the $Pr_{0.7}Ca_{0.3}Mn_{0.8}Cr_{0.2}O_3$ sample [the units for $A(T)$, $B(T)$ and $C(T)$ are T^2 kg/J, T^4 kg^3/J^3 and T^6 kg^5/J^5, respectively] and experimental and theoretical magnetic entropy changes ΔS for the $Pr_{0.7}Ca_{0.3}Mn_{0.8}Cr_{0.2}O_3$ at magnetic fields of 1–5

$$\frac{\mu_0 H}{M} = A(T) + B(T) \times M^2 + C(T) \times M^4 \qquad (7)$$

These Landau coefficients A, B and C are identified from polynomial fits of the Arrott plots to Eq. (7) which are displayed in Fig. 8. According to Inoue–Shimizu model [77], $A(T)$ is the inverse of the magnetic susceptibility, with a minimum at T_C. The sign of B can be used to distinguish the magnetic transitions order, as it indicates the first-order transition ($B < 0$) or the second-order transition ($B > 0$). As shown in Fig. 8, $B(T)$ has a positive value when $A(T)$ reaches the minimum, denoting a second-order transition in $Pr_{0.7}Ca_{0.3}Mn_{0.8}Cr_{0.2}O_3$. The corresponding magnetic entropy can be obtained by differentiating Gibbs free energy with respect to temperature as:

$$
\begin{aligned}
\Delta S(T, \mu_0 H) &= S(T,\ 0) - S(T, \mu_0 H) \\
&= -\frac{1}{2}A'(T) \times (M_0^2 - M^2) - \frac{1}{4}B'(T) \times (M_0^4 - M^4) \\
&\quad - \frac{1}{6}C'(T) \times (M_0^6 - M^6)
\end{aligned}
$$

$$(8)$$

Thus, $\Delta S(T)$ can be calculated using Eq. (8) where $A'(T)$, $B'(T)$ and $C'(T)$ are the temperature derivatives of Landau coefficients. The value of M_0 can be obtained by extrapolating the magnetization at $\mu_0 H = 0$. As shown in Fig. 8, the red lines represent the calculated magnetic entropy change by the Landau theory and the symbols represent the experimental data at $\mu_0 H = 1, 2, 3, 4$ and 5 T, respectively. The plot exactly matches the experimental data above Curie temperature. However, this mean field approximation cannot interpret the results below T_C. The obtained results are similar to that observed in hole-doped manganites where Landau analysis nicely corroborated the experimental data for polycrystalline compound [78]. This agreement considering the fact that the present model does not take into account the influence of the Jahn–Teller effect and exchange interactions on the magnetic properties of manganites. The analysis clearly reveals the importance of magnetoelastic coupling and electron interaction in understanding the magnetocaloric properties of lanthanum manganites [11, 17, 78].

Conclusions

In summary, the polycrystalline compounds were prepared by the conventional solid-state reaction method. X-ray results indicated that all the samples are single phase and crystallize in the orthorhombic system with Pnma space group. Magnetocaloric effect and transition order were investigated by using magnetization measurements. The 20% Cr substitution drives the system from charge-ordered state to ferromagnetic one. Our results indicate that chromium substitution in charge-ordered manganites is one of the possible ways to enhance magnetocaloric effect in these complex oxides and it is certainly better than doping at Mn site in ferromagnetic manganites. Banerjee criterion, the universal behavior and Landau analysis reveal a second-order transition in $Pr_{0.7}Ca_{0.3}Mn_{0.8}Cr_{0.2}O_3$. Comparison between the calculated and experimental values of entropy changes indicates a potential transition of magnetic interaction in the vicinity of T_C. The Cr-substituted material possesses some appropriate properties for a good candidate as magnetic cooling in a low temperature range.

References

1. Gschneidner KA, Pecharsky VK. Magnetocaloric materials. Annu Rev. 2000;30(1):387–429.
2. Barclay JA. Active and passive magnetic regenerators in gas/magnetic refrigerators. J Alloys Compd. 1994;207–208:355–61.
3. M'nassri R, Cheikhrouhou A. Magnetocaloric properties in ordered double-perovskite $Ba_2Fe_{1-x}Cr_xMoO_6$ ($0 \le x \le 1$). J Korean Phys Soc. 2014;64(6):879–85.
4. Tishin AM, Spichkin YI. The magnetocaloric effect and its applications. Bristol: Institute of Physics Publishing; 2003.
5. Pecharsky VK, Gschneidner KA Jr. Giant magnetocaloric effect in $Gd_5(Si_2Ge_2)$. Phys Rev Lett. 1997;78(23):4494–7.
6. Beltran-Lopez JF, Sazatornil M, Palacios E, Burriel R. Application of simulations to thermodynamic properties of materials for magnetic refrigeration. J Therm Anal. 2016;125(2):579–83.
7. M'nassri R, Cheikhrouhou A. Magnetocaloric effect in $LaFe_{10.7}Co_{0.8}Si_{1.5}$ compound near room temperature. J Supercond Nov Magn. 2013;27(4):1059–64.
8. Swamy NK, Kumar NP, Gupta M, Samatham SS, Ganesan V, Malik V, et al. Structural, magnetic, thermodynamic, and transport properties of A-site disordered $Nd_{0.3}Sm_{0.2}Sr_{0.5}MnO_3$. J Therm Anal Calorim. 2014;122(1):145–50.
9. Shen BG, Sun JR, Hu FX, Zhang HW, Cheng ZH. Recent progress in exploring magnetocaloric materials. Adv Mater. 2009;21(45):4545–64.
10. M'nassri R. Enhancement of refrigeration capacity and table-like magnetocaloric effect in $LaFe_{10.7}Co_{0.8}Si_{1.5}/La_{0.6}Pr_{0.4}Fe_{10.7}Co_{0.8}Si_{1.5}$ composite. J Supercond Nov Magn. 2015;29(1):207–13.
11. M'nassri R, Boudjada NC, Cheikhrouhou A. Nearly constant magnetic entropy change involving the enhancement of refrigerant capacity in $(La_{0.6}Ba_{0.2}Sr_{0.2}MnO_3)_{1-x}/(Co_2O_3)_x$ composite. Ceram Int. 2016;42(6):7447–54.
12. Phan M-H, Yu S-C. Review of the magnetocaloric effect in manganite materials. J Magn Magn Mater. 2007;308(2):325–40.
13. M'nassri R, Boudjada NC, Cheikhrouhou A. Impact of sintering temperature on the magnetic and magnetocaloric properties in $Pr_{0.5}Eu_{0.1}Sr_{0.4}MnO_3$ manganites. J Alloys Compd. 2015;626:20–8.
14. Selmi A, M'nassri R, Cheikhrouhou-Koubaa W, Boudjada NC, Cheikhrouhou A. Effects of partial Mn-substitution on magnetic and magnetocaloric properties in $Pr_{0.7}Ca_{0.3}Mn_{0.95}X_{0.05}O_3$ (Cr, Ni, Co and Fe) manganites. J Alloys Compd. 2015;619:627–33.

15. Lampen P, Puri A, Phan M-H, Srikanth H. Structure, magnetic, and magnetocaloric properties of amorphous and crystalline La$_{0.4}$Ca$_{0.6}$MnO$_{3+\delta}$ nanoparticles. J Alloys Compd. 2012;512(1):94–9.
16. Choura Maatar S, M'nassri R, Cheikhrouhou Koubaa W, Koubaa M, Cheikhrouhou A. Structural, magnetic and magnetocaloric properties of La$_{0.8}$Ca$_{0.2-x}$Na$_x$MnO$_3$ manganites (0 ≤ x ≤ 0.2). J Solid State Chem. 2015;225:83–8.
17. M'nassri R, Cheikhrouhou-Koubaa W, Boudjada NC, Cheikhrouhou A. Effect of barium-deficiency on the structural, magnetic, and magnetocaloric properties of La$_{0.6}$Sr$_{0.2}$Ba$_{0.2-x}$□$_x$MnO$_3$ (0 ≤ x ≤ 0.15). J Appl Phys. 2013;113(7):073905.
18. Ravi S, Karthikeyan A. Effect of calcination temperature on La$_{0.7}$Sr$_{0.3}$MnO$_3$ nanoparticles synthesized with modified sol–gel route. Phys Proc. 2014;54:45–54.
19. Ding Y, Haskel D, Tseng Y-C, Kaneshita E, van Veenendaal M, Mitchell JF, et al. Pressure-induced magnetic transition in manganite (La$_{0.75}$Ca$_{0.25}$MnO$_3$). Phys Rev Lett. 2009;102(23):237201.
20. M'nassri R, Cheikhrouhou A. Magnetocaloric effect in different impurity doped La$_{0.67}$Ca$_{0.33}$MnO$_3$ composite. J Supercond Nov Magn. 2013;27(2):421–5.
21. Selmi A, M'nassri R, Cheikhrouhou-Koubaa W, Boudjada NC, Cheikhrouhou A. Influence of transition metal doping (Fe Co, Ni and Cr) on magnetic and magnetocaloric properties of Pr$_{0.7}$Ca$_{0.3}$MnO$_3$ manganites. Ceram Int. 2015;41(8):10177–84.
22. Zener C. Interaction between the d-shells in the transition metals. II. Ferromagnetic compounds of manganese with perovskite structure. Phys Rev B. 1951;82(3):403–5.
23. Millis AJ. Cooperative Jahn–Teller effect and electron-phonon coupling inLa$_{1-x}$A$_x$MnO$_3$. Phys Rev B. 1996;53(13):8434–41.
24. Mori S, Chen CH, Cheong S-W. Paired and unpaired charge stripes in the ferromagnetic phase of La$_{0.5}$Ca$_{0.5}$MnO$_3$. Phys Rev Lett. 1998;81(18):3972–5.
25. Gor'kov LP, Kresin VZ. Mixed-valence manganites: fundamentals and main properties. Phys Rep. 2004;400(3):149–208.
26. Kim H-J, Yoo S-I. Enhanced low field magnetoresistance in La$_{0.7}$Sr$_{0.3}$MnO$_3$–La$_2$O$_3$ composites. J Alloys Compd. 2012;521:30–4.
27. Guo ZB, Du YW, Zhu JS, Huang H, Ding WP, Feng D. Large magnetic entropy change in perovskite-type manganese oxides. Phys Rev Lett. 1997;78(6):1142–5.
28. Kumar VS, Mahendiran R. Effect of impurity doping at the Mn-site on magnetocaloric effect in Pr$_{0.6}$Ca$_{0.4}$Mn$_{0.96}$B$_{0.04}$O$_3$ (B = Al, Fe, Cr, Ni Co, and Ru). J Appl Phys. 2011;109(2):023903.
29. Hébert S, Maignan A, Hardy V, Martin C, Hervieu M, Raveau B, et al. Magnetization and resistivity steps in the phase separated Pr Ca Mn Ni O manganites. Eur Phys J B. 2002;29(3):419–24.
30. Mahendiran R, Maignan A, Hervieu M, Martin C, Raveau B. Anomalous magnetotransport in Pr$_{0.5}$Ca$_{0.5}$Mn$_{0.99}$Cr$_{0.01}$O$_3$. Appl Phys Lett. 2000;77(10):1517.
31. Ikebe M, Fujishiro H, Kanoh S, Yamazaki H. Lattice effect on ferromagnetic-metal phase transition in Pr$_{0.65}$Ca$_{0.35}$(Mn$_{1-z}$Co$_z$)O$_3$ and Pr$_{0.65}$Ca$_{0.35}$(Mn$_{1-z}$Cr$_z$)O$_3$. J Magn Magn Mater. 2004;272–276:1798–9.
32. Markovich V, Fita I, Puzniak R, Martin C, Wisniewski A, Yaicle C, et al. Instability of magnetism in Pr$_{0.5}$Ca$_{0.5}$Mn$_{1-x}$Cr$_x$O$_3$ (x = 0.015,0.03): competition between pressure and thermal cycling effects. Phys Rev B 2006;73(22):224423.
33. Jonker GH. Magnetic compounds with perovskite structure IV conducting and non-conducting compounds. Physica 1956;22(6–12):707–22.
34. Selmi A, Bettaibi A, Rahmouni H, M'nassri R, Boudjada NC, Chiekhrouhou A, et al. Physical properties of 20% Cr-doped Pr$_{0.7}$Ca$_{0.3}$MnO$_3$ perovskite. Ceram Int. 2015;41(9):11221–7.
35. Kuo JH, Anderson HU, Sparlin DM. Oxidation-reduction behavior of undoped and Sr-doped LaMnO$_3$ nonstoichiometry and defect structure. J Solid State Chem. 1989;83(1):52–60.
36. Ben Khlifa H, M'nassri R, Cheikhrouhou-Koubaa W, Hlil EK, Cheikhrouhou A. Effects of synthesis route on the structural, magnetic and magnetocaloric properties of Pr$_{0.8}$K$_{0.2}$MnO$_3$. Ceram Int. 2017;43(2):1853–61.
37. Rietveld HM. A profile refinement method for nuclear and magnetic structures. J Appl Cryst. 1969;2(2):65–71.
38. Roisnel, T., Rodriguez-Carvajal, J. Computer program FULLPROF, LLB-LCSIM, 2003.
39. Turpu GR, Gupta A, Reddy KR. Magnetic field-induced transitions in La$_{0.42}$Eu$_{0.25}$Ca$_{0.33}$MnO$_3$ perovskite manganite. J Phys D Appl Phys. 2009;42(14):145004.
40. Mahendiran R, Maignan A, Hébert S, Martin C, Hervieu M, Raveau B, et al. Ultrasharp magnetization steps in perovskite manganites. Phys Rev Lett. 2002;89(28):286602.
41. Heilman AK, Xue YY, Lorenz B, Campbell BJ, Cmaidalka J, Meng RL, et al. Distinct insulating state below the Curie point in Pr$_{0.7}$Ba$_{0.3}$MnO$_3$. Phys Rev B. 2002;65(21):214423.
42. M'nassri R, Cheikhrouhou-Koubaa W, Boudjada N, Cheikhrouhou A. Magnetocaloric effects in Pr$_{0.6-x}$Er$_x$Sr$_{0.4}$MnO$_3$ (0.0 ≤ x ≤ 0.2) manganese oxides. J Supercond Nov Magn. 2012;26(5):1429–35.
43. Mahendiran R, Hervieu M, Maignan A, Martin C, Raveau B. Coexistence of ferromagnetism and charge ordering in Pr$_{0.5}$Ca$_{0.5}$Mn$_{1-x}$Cr$_x$O$_3$. Solid State Commun. 2000;114(8):429–33.
44. Şen C, Alvarez G, Dagotto E. Competing ferromagnetic and charge-ordered states in models for manganites: the origin of the colossal magnetoresistance effect. Phys Rev Lett. 2007;98(12):127202.
45. Muthuselvam IP, Bhowmik RN. Grain size dependent magnetization, electrical resistivity and magnetoresistance in mechanically milled La$_{0.67}$Sr$_{0.33}$MnO$_3$. J Alloys Compd. 2012;511(1):22–30.
46. Srivastava SK, Ravi S. Magnetic properties of transition metal substituted La$_{0.85}$Ag$_{0.15}$Mn$_{1-y}$M$_y$O$_3$ compounds (M = Co, Cr and Al). J Magn Magn Mater. 2009;321(24):4072–80.
47. Ling L, Fan J, Pi L, Tan S, Zhang Y. Effect of magnetism and average radius at A-site on in (, Pr, Gd, Dy) system. Solid State Commun. 2008;145(1–2):11–4.
48. M'nassri R, Cheikhrouhou-Koubaa W, Koubaa M, Cheikhrouhou A. Effect of strontium substitution on the physical properties of Nd$_{0.5}$Ca$_{0.5-x}$Sr$_x$MnO$_3$ (0.0 ≤ x ≤ 0.5) manganites. IOP Conf Ser Mater Sci Eng. 2012;28:012050.
49. Banerjee BK. On a generalised approach to first and second order magnetic transitions. Phys Lett. 1964;12(1):16–7.
50. Nair S, Banerjee A. The effect of Al substitution on charge ordered Pr$_{0.5}$Ca$_{0.5}$MnO$_3$: structure, magnetism and transport. J Phys: Condens Matter. 2004;16(46):8335–44.
51. Moutis N, Panagiotopoulos I, Pissas M, Niarchos D. Structural and magnetic properties of La$_{0.67}$(Ba$_x$Ca$_{1-x}$)$_{0.33}$MnO$_3$ perovskites(0 < ~x < ~1). Phys Rev B. 1999;59(2):1129–33.
52. Kim D, Zink BL, Hellman F, Coey JMD. Critical behavior of La$_{0.75}$Sr$_{0.25}$MnO$_3$. Phys Rev B. 2002;65(21):214424.
53. M'nassri R. Field dependence of magnetocaloric properties in La$_{0.6}$Pr$_{0.4}$Fe$_{10.7}$Co$_{0.8}$Si$_{1.5}$. J Supercond Novel Magn. 2014;27(7):1787–94.
54. Mahjoub S, Baazaoui M, M'nassri R, Rahmouni H, Boudjada NC, Oumezzine M. Effect of iron substitution on the structural, magnetic and magnetocaloric properties of Pr$_{0.6}$Ca$_{0.1}$Sr$_{0.3}$Mn$_{1-x}$Fe$_x$O$_3$ (0 ≤ x ≤ 0.075) manganites. J Alloys Compd. 2014;608:191–6.
55. Oumezzine E, Hcini S, Hlil E-K, Dhahri E, Oumezzine M. Effect of Ni-doping on structural, magnetic and magnetocaloric properties of La$_{0.6}$Pr$_{0.1}$Ba$_{0.3}$Mn$_{1-x}$Ni$_x$O$_3$ nanocrystalline manganites synthesized by Pechini sol–gel method. J Alloys Compd. 2014;615:553–60.

56. Barik SK, Krishnamoorthi C, Mahendiran R. Effect of Fe substitution on magnetocaloric effect in $La_{0.7}Sr_{0.3}Mn_{1-x}Fe_xO_3$ ($0.05 \leq x \leq 0.20$). J Magn Magn Mater. 2011;323(7):1015–21.

57. Sun Y, Tong W, Zhang Y. Large magnetic entropy change above 300 K in $La_{0.67}Sr_{0.33}Mn_{0.9}Cr_{0.1}O_3$. J Magn Magn Mater. 2001;232(3):205–8.

58. Hcini S, Boudard M, Zemni S, Oumezzine M. Effect of Fe-doping on structural, magnetic and magnetocaloric properties of $Nd_{0.67}Ba_{0.33}Mn_{1-x}Fe_xO_3$ manganites. Ceram Int. 2014;40(10):16041–50.

59. Nisha P, Savitha Pillai S, Varma MR, Suresh KG. Critical behavior and magnetocaloric effect in $La_{0.67}Ca_{0.33}Mn_{1-x}Cr_xO_3$ ($x = 0.1, 0.25$). Solid State Sci. 2012;14(1):40–7.

60. Oumezzine M, Peña O, Kallel S, Oumezzine M. Crossover of the magnetocaloric effect and its importance on the determination of the critical behaviour in the $La_{0.67}Ba_{0.33}Mn_{0.9}Cr_{0.1}O_3$ perovskite manganite. J Alloys Compd. 2012;539:116–23.

61. Franco V, Conde A. Scaling laws for the magnetocaloric effect in second order phase transitions: From physics to applications for the characterization of materials. Int J Refrigerat. 2010;33(3):465–73.

62. Franco V, Blázquez JS, Conde A. Field dependence of the magnetocaloric effect in materials with a second order phase transition: a master curve for the magnetic entropy change. Appl Phys Lett. 2006;89(22):222512.

63. Zhang L, Fan J, Tong W, Ling L, Pi L, Zhang Y. Scaling of the magnetic entropy change in spinel selenide $CuCr_2Se_4$. Phys B. 2012;407(17):3543–6.

64. Prida VM, Franco V, Vega V, Sánchez-Llamazares JL, Suñol JJ, Conde A, et al. Magnetocaloric effect in melt-spun FePd ribbon alloy with second order phase transition. J Alloys Compd. 2011;509(2):190–4.

65. Yang H, Zhu YH, Xian T, Jiang JL. Synthesis and magnetocaloric properties of $La_{0.7}Ca_{0.3}MnO_3$ nanoparticles with different sizes. J Alloys Compd. 2013;555(555):150–5.

66. Raju K, Pavan Kumar N, Venugopal Reddy P, Yoon DH. Influence of Eu doping on magnetocaloric behavior of $La_{0.67}Sr_{0.33}MnO_3$. Phys Lett A. 2015;379(16–17):1178–82.

67. Zhang XX, Wen GH, Wang FW, Wang WH, Yu CH, Wu GH. Magnetic entropy change in Fe-based compound $LaFe_{10.6}Si_{2.4}$. Appl Phys Lett. 2000;77(19):3072.

68. Kumar Swamy N, Pavan Kumar N, Reddy PV, Gupta M, Samatham SS, Venkateshwarulu D, et al. Specific heat and magnetocaloric effect studies in multiferroic $YMnO_3$. J Therm Anal Calorim. 2014;119(2):1191–8.

69. Thaljaoui R, Boujelben W, Pękała K, Pękała M, Cheikhrouhou-Koubaa W, Cheikhrouhou A. Magnetocaloric study of monovalent-doped manganites $Pr_{0.6}Sr_{0.4-x}Na_xMnO_3$ ($x = 0$–0.2). J Mater Sci. 2013;48(11):3894–903.

70. Thaljaoui R, Boujelben W, Pękała M, Pękała K, Fagnard J-F, Vanderbemden P, et al. Magnetocaloric effect of monovalent K doped manganites $Pr_{0.6}Sr_{0.4-x}K_xMnO_3$ ($x = 0$–0.2). J Magn Magn Mater. 2014;352:6–12.

71. Law JY, Ramanujan RV, Franco V. Tunable Curie temperatures in Gd alloyed Fe–B–Cr magnetocaloric materials. J Alloys Compd. 2010;508(1):14–9.

72. Mbarek H, M'nasri R, Cheikhrouhou-Koubaa W, Cheikhrouhou A. Magnetocaloric effect near room temperature in $(1-y)La_{0.8}Ca_{0.05}K_{0.15}MnO_3/yLa_{0.8}K_{0.2}MnO_3$ composites. Phys Status Solidi (a). 2014;211(5):975–9.

73. Franco V, Blázquez JS, Conde A. The influence of Co addition on the magnetocaloric effect of Nanoperm-type amorphous alloys. J Appl Phys. 2006;100(6):064307.

74. Phan T-L, Zhang P, Thanh TD, Yu SC. Crossover from first-order to second-order phase transitions and magnetocaloric effect in $La_{0.7}Ca_{0.3}Mn_{0.91}Ni_{0.09}O_3$. J Appl Phys. 2014;115(17):17A912.

75. Caballero-Flores R, Franco V, Conde A, Kiss LF. Influence of the demagnetizing field on the determination of the magnetocaloric effect from magnetization curves. J Appl Phys. 2009;105(7):07A919.

76. Franco V, Caballero-Flores R, Conde A, Dong QY, Zhang HW. The influence of a minority magnetic phase on the field dependence of the magnetocaloric effect. J Magn Magn Mater. 2009;321(9):1115–20.

77. Inoue J, Shimizu M. Volume dependence of the first-order transition temperature for RCo_2 compounds. J Phys F Metal Phys. 1982;12(8):1811–9.

78. Amaral JS, Reis MS, Amaral VS, Mendonc TM, Araunjo JP, Sa MA, Tavares PB, Vieir JM. Magnetocaloric effect in Er- and Eu-substituted ferromagnetic La–Sr manganites. J Magn Magn Mater. 2005;290–291:686–9.